FORSCHUNGSZENTRUM JÜLICH GmbH

Institut für Kernphysik

Response Function of the Trigger Scintillation Detector for the COSY 11 Installation

Pawel Moskal

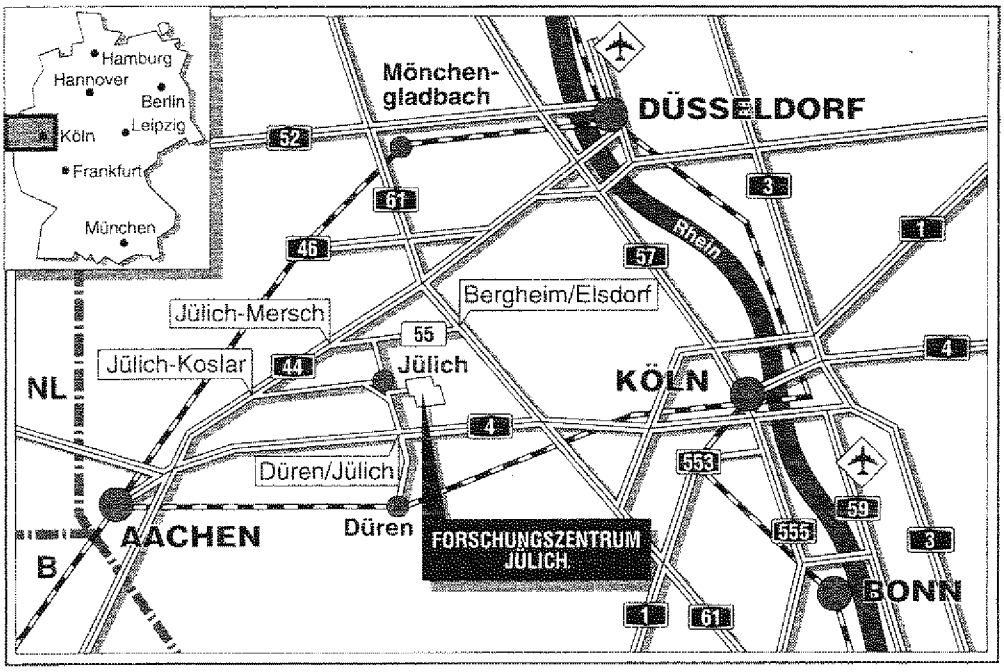

Berichte des Forschungszentrums Jülich ; 2825
ISSN 0944-2952
Institut für Kernphysik Jül-2825

Zu beziehen durch: Forschungszentrum Jülich GmbH · Zentralbibliothek
D-52425 Jülich · Bundesrepublik Deutschland
Telefon: 02461/61-6102 · Telefax: 02461/61-6103 · Telex: 833556-70 kfa d

Response Function of the Trigger Scintillation Detector for the COSY 11 Installation

Pawel Moskal

Contents

Introduction

Thorough investigations carried out over many years revealed, that the hadronic matter is certainly much richer than the simple constituent quark model expectation with only three quark and quark - antiquark hadrons. The QCD theory predicts the existence of hadronic objects, other than the known baryons and mesons, like glueballs and hybrids ($q\overline{q}g$). Presently available data, however, does not provide sufficient information to judge, for instance, whether $f_o(975)$ and $a_o(980)$ mesons reveal $q\overline{q}$, $qq\overline{qq}$ or $K\overline{K}$ molecular structure . Their small two-photon partial width $\Gamma_{\gamma\gamma}$ and a very narrow full width [2] still remain unexplained. Further, there exists some recent theoretical predictions [1] that $s\overline{s}$ quarks constitute only 50% of the $\phi(1020)$ meson, which is generally regarded to possess pure $s\overline{s}$ structure. However, so far this is not confirmed experimentally. Equally interesting is a discussion of the gluon content of eg. the $\eta'(958)$ meson [1]. A few attempts were made to predict theoretical glueball masses, but the results are model dependant [2]. Thus, investigations which can prove the existence of the exotic quark states are presently of significant interest in medium energy physics.

In order to find an answer to some of the above mentioned problems the detection system, sketched in Fig. 0.1, has been designed. Soon it is to be installed in the cooler synchrotron ring (COSY) at Jülich, which will

provide a high quality proton beam with proton momenta up to 3.3 GeV/c. Experiments are planned to allow the study of the structure of resonances in $pp \rightarrow ppM^0$ and $pp \rightarrow pnM^+$ reactions with meson masses up to the meson $\phi(1020)$ and also investigations on $meson - meson$ or $meson - nucleon$ final state interaction via reactions of the type $pp \rightarrow ppM_1M_2$.

The aim of this work is to test the response of a scintillation detector (indicated in Fig. 0.1 as S1) to ionizing particles. This counter, consisting of sixteen detection modules, will serve as a trigger of the whole detection system. Thus the time resolution as well as a signal amplitude variation with respect to a hit position is of a special interest. The former because this detector will be used as a start counter for the time of flight measurement, the latter as it will provide energy loss measurements of the particles.

The present work is divided into two parts. In the first one the main stages of a signal production by scintillation counters are considered. In the second one the first chapter presents measurements of the characteristics of the photomultiplier, whereas the second one contains a description of the experimental set-ups as well as the method of data evaluation. The final chapter in turn presents the main characteristics of the considered detector.

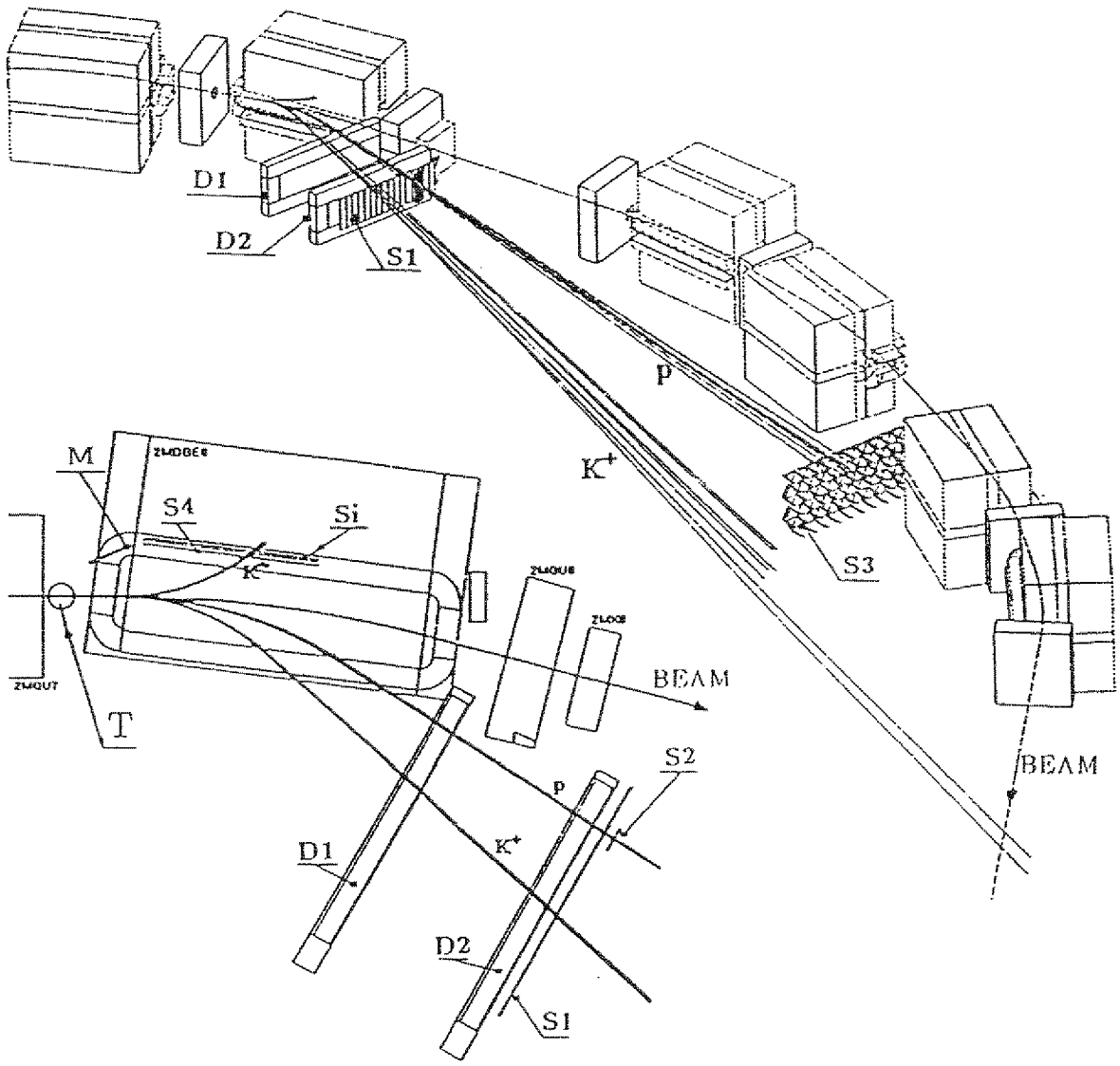

Figure 0.1 Schematic drawing of the COSY - 11 (E-5) experimental set-up. The trajectories shown are for the $pp \rightarrow pp K^+ K^-$ reaction, at a beam momentum 2 MeV above a threshold.

D1,D2 ..... drift chambers with an active area of $43 \times 168\,cm^2$,
S1,S2,S3,S4 ..... scintillation counters with an active area of, $45 \times 160\,cm^2$, $46 \times 21.6\,cm^2$, $150 \times 200\,cm^2$, $6 \times 110\,cm^2$, respectively,
Si ..... silicon pad array with an active area of $5.8 \times 105\,cm^2$,
M ..... monitor detector (silicon pad array - $5.8 \times 21\,cm^2$),
T ..... claster target,
(Courtesy M. Rook and D. Grzonka)

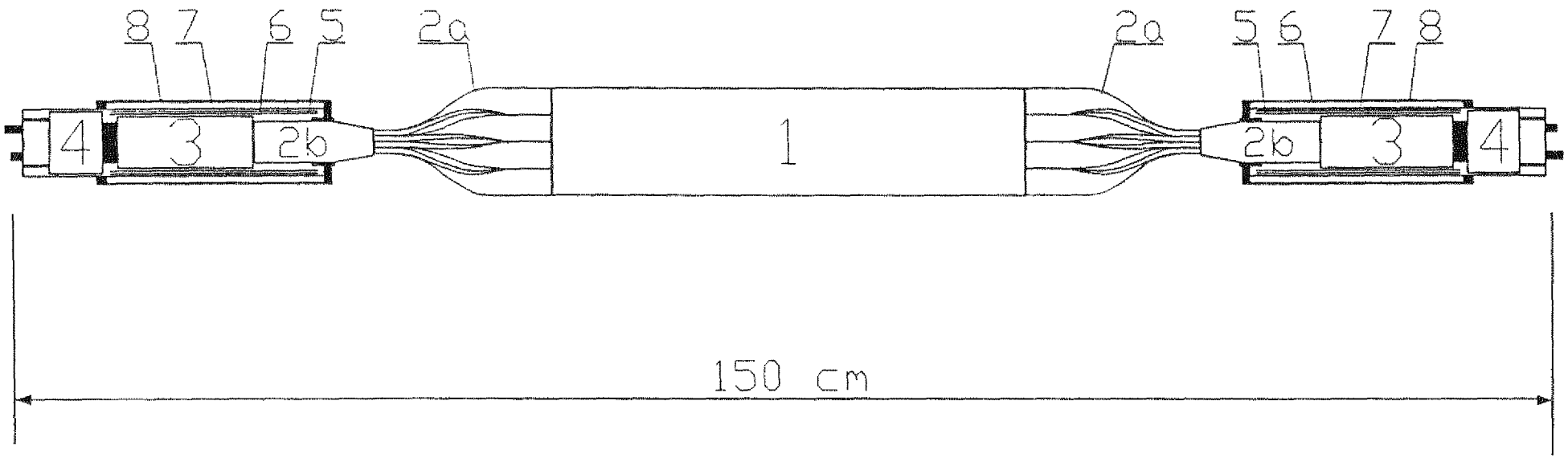

Figure 0.2 Schematic diagram of a separate module of the S1 detector.

1 ..... scintillator BC-404 of dimensions 450 x 100 x 4 mm^3,
2a ..... twisted strip light quide made of GS233 Röhm plexiglass,
2b ..... cylindrical light guide,
3 ..... photomultiplier EMI 9954B,
4 ..... photomultiplier base (voltage divider network) type 4244,
5 ..... capton foil,
6 ..... mu metal,
7 ..... plastic housing,
8 ..... iron protective shield

Chapter 1

The detection module operation

There exists a certain kind of material, scintillator, which emits flashes of light when exposed to radiation. This peculiarity enables to make use of such materials in particle and radiation detection. The very early technique, first applied by Crooks in 1903, was based on the observation of light flashes by means of a microscope in a darkened room. This, however, was exeedingly laborious and thus not very popular. In 1944 the photomultiplier replaced the human eye making very efficient and reliable particle detection possible. Since that time for almost fifty years scintillation counters have been successfully used in a very wide range of nuclear and particle physics experiments.

The basic processes involved in the particle detection are as follows : A charged particle, when hitting the scintillator, deposits therein a part of its energy, through the ionization or excitation of the electrons to the higher molecular levels. Subsequent deexcitation processes result in photon production. A fraction of emitted photons travels to the edge of the scintillator, from where they are transported via the light guide to the photomultiplier. The photomultiplier first converts the light into a weak photoelectron current, and afterwards amplifies it, so that the output signal can be analyzed by the electronics system.

1.1 Mechanism of the light pulse production in a plastic scintillator

Table 1. Some physical properties of BC-404 plastic scintillator [3]

Density [g/cm^3]	Refractive index	Light output (% Anthracene)	Wavelength of maximum emission [nm]	Base
1.032	1.581	68	408	PVT
Rise time [ns]	**Pulse width FWHM [ns]**	**Decay constant main component [ns]**	**Bulk light attenuation [cm]**	**Softening point [^{0}C]**
0.7	2.2	1.8	120	75

The fluorescence process in organic scintillators arises from radiative transitions in a single molecule and does not depend on the physical state of the material. In such a molecule the valence electron orbitals combine to form π - electron energy levels. The radiative transitions among them account for the scintillations. The π - electron system is schematically shown in Fig. 1.1. Dashed lines indicate vibrational sub-levels superimposed on each of the electro-magnetic levels.

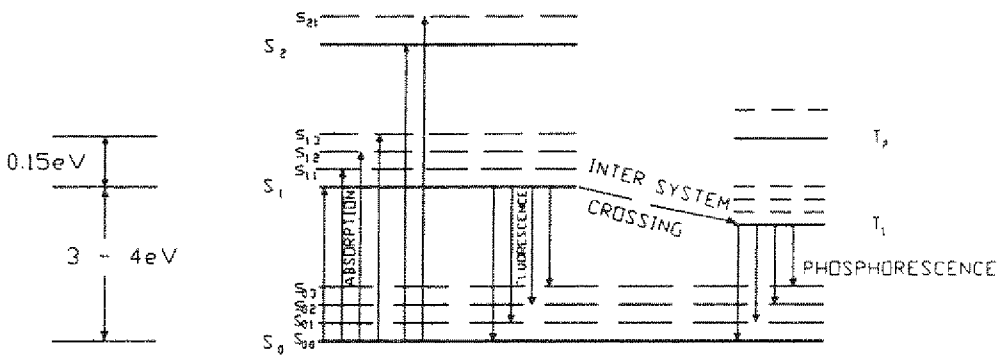

Figure 1.1 π - **Electronic energy levels of an organic molecule.** S_0, **ground state.** S_1, S_2, **excited singlet states.** T_1, T_2, **excited triplet states.** S_{00}, S_{01} ... **etc. vibrational sub-levels [4]**

BC - 404 is a ternary plastic scintillator. Ternary means that two admixtures are dissolved in the base material. The base of this scintillator is polyvinyltoluene. It scintillates as pure material, but its light output is relatively low. This is considerably improved by dissolving therein a small amount (a few percent) of an aromatic compound called primary solute. However, such a solution can not be used in large quantities, because of a strong light absorption. Second additive (secondary solute) allows to get rid of this disadvantage by shifting the emitted light to a longer wavelength.

In ternary scintillators the concentration of the admixtures is so small, that their excitation by an ionizing particle can be neglected. Thus, at first, the particle deposit its energy in the base. Next this energy may be transferred to the solute, both radiatively and non-radiatively. However, because of the very low concentration of the secondary solute, this transfer occurs mostly between the base molecule and primary admixture. The additive is chosen, so that the energy of its first excited level is lower than the energy of the first excited level of the base molecule. (see Fig. 1.2)

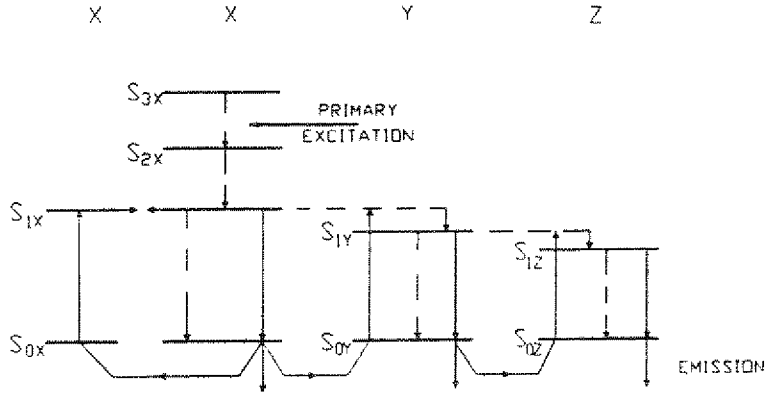

Figure 1.2 The scintillation process in a ternary organic solution scintillator. (X = solvent(base), Y = primary solute, Z = secondary solute). Continuous lines – radiative transitions, dashed lines – non-radiative transitions [4]

Further , the excitation energy from the primary solute is transferred to the secondary solute called wavelength shifter. A proper choice of the

latter allows to match the scintillator emission spectrum to the sensitiveness of the photomultiplier. The energy of the photons emitted by the secondary solute is very low in comparison with the first excited state in polyvinyltoluene. Thus, these photons are not able to excite the molecules of the base. This makes the ternary solution transparent to its own radiation, and allows to use samples of large dimensions. The light emission spectrum of the BC-404 scintillator is shown in Figure 1.3.

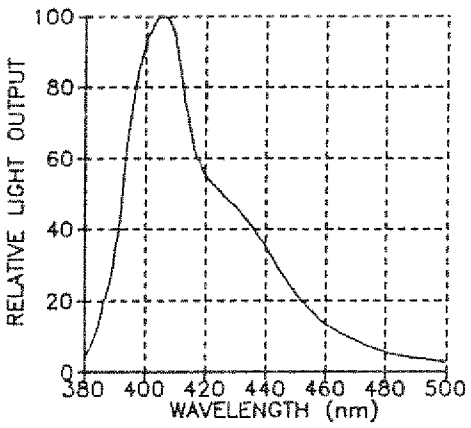

Figure 1.3 Normalized emission spectrum of the BC-404 scintillator [3]

The radiationless processes such as the internal conversion from the higher excited states of the solvent, or non-radiative intermolecular energy transfer are much faster then the radiative processes [5]. For that reason the signal shape is determined by the light emission from a wavelength shifter and by the radiative energy transfers. M. Moszynski and H. Bengston [6] proposed the following equation to describe the light pulse shape from the ternary scintillator :

$$i(t) = f_G(t, \sigma, \mu) \cdot (e^{-t/\tau} - e^{-t/\tau_1}) \qquad (1.1)$$

where $i(t)$ is the light intensity, $f_G(t)$ is a Gaussian function describing the rate of the energy transfer from a detected particle to the primary solute, this term reflects the final rise time of the signal. Term e^{-t/τ_1} describes the energy transfer to the wavelength shifter and $e^{-t/\tau}$ describes the final

light emission. Therefore the pulse is characterized by four parameters $\mu, \sigma, \tau, \tau_1$, which can be found by fitting the equation to the measured signal. Of course the photomultiplier response has to be taken into account.

However, equation 1.1 may be applied only to small samples, where the light pulse shape depends only on the composition of the scintillator. In large scintillators the pulse shape is affected by the light collection, the self-absorbtion and re-emision processes. Their influence manifests mainly in shifting the light to the longer wavelength and in increasing the decay time constant. Thus equation 1.1 is modified as follows:

$$i(t) = i_s(t) \cdot e^{-t/\delta} \cdot e^{-t/\tau_2} \tag{1.2}$$

where $i_s(t)$ is the light pulse from a small sample (eq. 1.1), $e^{-t/\delta}$ is associated with photon transit time in a scintillator, and the term e^{-t/τ_2} accouts for the self-absorbtion and re-emission process [7].

1.2 The light collection process

Table 2. Physical properties of GS233 Röhm plexiglass [8]

Material	Refractive index	Bulk light attenuation length [cm]	Density $[g/cm^3]$
Polymethylmethacrylat	1.491	600	1.18

In a scintillator the photon emission is isotropic in all directions. For photon angles above the Brewster angle all photons are totally reflected. The remainder leaves the scintillator or is partially reflected according to the Fresnel's rules. The Brewster angle is given by

$$\theta_B = arc\ sin(\frac{n_{out}}{n_{scint}}) \tag{1.3}$$

with n_{scint} - refrective index of the scintillator and n_{out} - refrective index of the surrounding medium.

In a symmetrical scintillator the totally reflected photon may reach each surface, provided that it is not absorbed within the material. Thus, connecting a chosen scintillator edge to another body of comparable reflective index one can guide the light to the required place. Among the presently used light guides a so called twisted strips one (see Fig. 0.2) possesses optimum light collection property [9]. It consists of separate strips glued on to the edge of the scintillator and twisted 90^0 so that they can fit the cylindrical photomultiplier shape.

Two practical rules allow to minimize the photons loss. Firstly, the cross sectional area of the light guide should never decrease. If it is the case then only a fraction of light, equals to the ratio of output to the input area, can be transferred. Secondly, a bend radius should be at least ten times larger than the thickness of the body. Equally important is the light guide transmission of the fluorescence light from the scintillator. The transmission of the GS233 plexiglass together with the BC-404 scintillator emission spectrum is shown below.

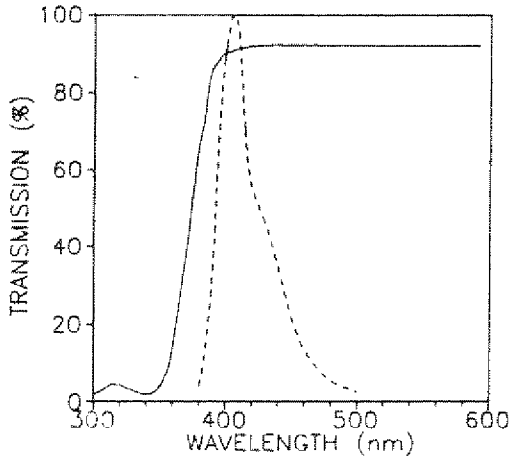

continuous line :
transmission spectrum

dashed line :
BC-404 emission spectrum

Figure 1.4 Transmission spectrum of the GS233 plexiglass [10] versus emission spectrum of the BC-404 scintillator

The whole scintillator module has to be enclosed in a light-tight envelope. The suitable covering may improve the collection property. However, the best would be to leave a layer of air surrounding the scintillator in or-

der to maximize the total internal reflections. In the present case the scintillator and the light guides are wrapped in aluminium foil, whose reflectivity for the light emitted by BC-404 material amounts to $\sim 90\%$ (see Fig. 1.5). Taking into account that on the average photons make 10 to 20 reflections before reaching the photocathode one can roughly estimate that only a few per cent of the photons, collected at the photocathode, originte from the external reflections.

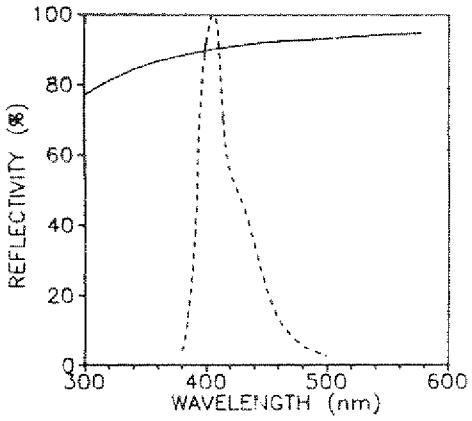

continuous line :
aluminium reflectivity

dashed line :
BC-404 emission spectrum

Figure 1.5 The aluminium reflectivity [13]

Thus primarily three factors influence the light collection efficiency. These are: the total internal reflection angle, the quality of the surfaces and the bulk light attenuation length, where the last is defined as the length after which the number of photons is diminished by a factor e^{-1}.

The longer the scintillator, the larger are the variations in the signal height over its volume. However, from this fact one can make a rough determination of the hit position of the detected particle.

1.3 Photomultiplier

Table 3. Characteristics of the 9954B EMI photomultiplier [11]

Photocathode type	QE% peak	Dynode material	Transit time [ns]	Typical gain
bialkali	26	BeCu	41	$6 \cdot 10^6$

The photomultiplier serves as a converter of the weak scintillation pulse into an electrical signal. Its operation may be considered as three subsequent processes. The photon convertion into a weak photoelectron current, the collection of the photoelectrons on the first multiplier dynode and the signal amplification by the multiplier structure.

1.3.1 The photoemission and electron collection processes

The incident light is partially absorbed in the photosensitive material deposited on the inside of the photomultiplier glass window. The captured photon transfers its entire energy to an encountered electron. Travelling to the boundary this electron will suffer an energy loss due to electron - electron collisions. In order to leave the photocathode it has to reach the surface with sufficient energy to overcome the potential barrier, which always exists at any interface between material and vacuum. The finite potential barrier imposes a minimum energy on the incoming photons. This is reflected in the long wavelenght cutoff of the photocathode efficiency (see Fig. 1.6). The cut in the short wavelenght is caused by the window material.

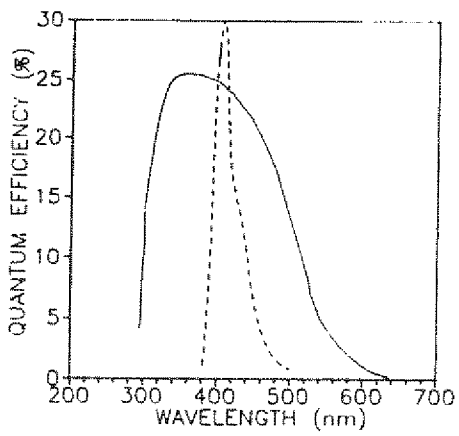

continuous line :
photocathode Q.E.

dashed line :
BC-404 emission spectrum

Figure 1.6 Quantum efficiency of a Bialkali photocathode [11] versus BC-404 emission spectrum

For some semiconductor material the "work function" is as low as 1.5 eV. The energy of the fluorescence light is about 3 - 4 eV (see Fig. 1.1).

Therefore, the depth at which electrons may originate and still escape from the material is about 25 nm [12]. A photocathode of this thickness may absorb no more than half of the incident light.

A number of large significance in scintillation counting is the photocathode quantum efficiency. It is defined as the ratio of the number of photoelectrons produced to the number of incident photons. The quantum efficiency is a function, which is strongly dependent on the light energy (see Fig. 1.6).

After emission from the photocathode the electrons travel, in a suitably designed electric field, towards the first dynode of the multiplier section. The time of flight of photoelectrons depends on the point in the photocathode, in which they originated (see Fig. 1.7). These differences are the main source of the spread of a transit time through the photomultiplier. Their are minimized, to some extent, by large distance and very high voltage between the photocathode and the first dynode in comparison with interdynode distances and voltages, respectively.

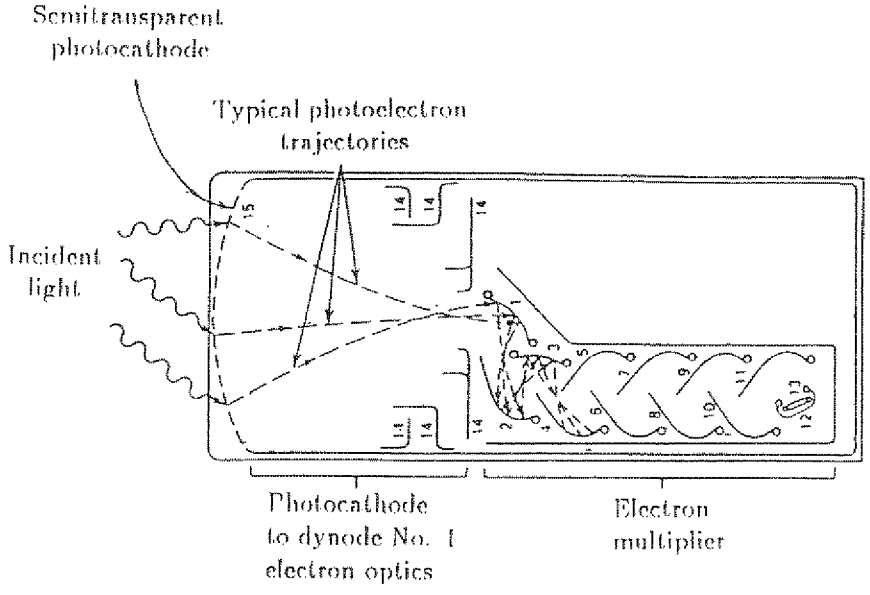

Figure 1.7 Basic elements of a photomultiplier tube (From [12])
1 - 12 — Dynodes, 13 — Anode,
14 — Focusing electrodes, 15 — Photocathode

1.3.2 The electron multiplication

The first multiplier dynode is held at a positive potential of several hundered volts with respect to the photocathode. Thus the electron impinging onto it may create in the order of one hundered new electrons. However, only a few of them manage to escape.

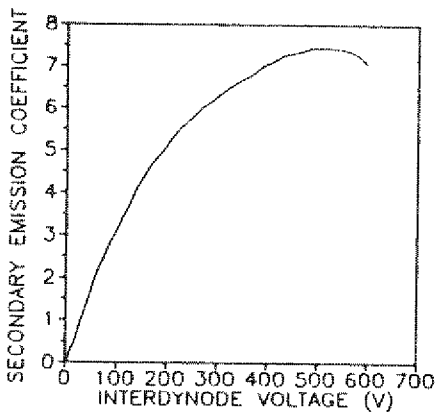

Figure 1.8 Secondary emission coefficient versus energy of the primary electron for BeCu material [13]

The secondary electrons, leaving the first dynode, are guided by an electrostatic field to the second one, where the process is repeated. The overall photomultiplier gain depends essentially on the number of dynodes and the secondary emission coefficient.

$$G = \delta_1 \cdot \delta_2 \cdot \ldots \cdot \delta_n \quad , \tag{1.4}$$

where δ - secondary emission factor, with typical δ value of ~ 5,
n - number of dynodes.

The δ is determined by the incident electron energy, which is proportional to the potential difference between the dynodes.

$$\delta = \mathrm{k} \cdot V_d$$

Assuming that the voltage is equally divided among the dynodes, the

overall gain is then given by:

$$G = (k \cdot V_d)^n = (\frac{k \cdot V}{n})^n \tag{1.5}$$

with V being the overall supplied voltage.

The expression

$$\frac{dG}{G} = n \cdot \frac{dV}{V} \tag{1.6}$$

derived from equation 1.5 shows the gain variation with respect to the applied voltage. One can see that this is a very strong dependence. A one per cent change in voltage may cause more than a ten per cent change in gain depending on the number of dynodes.

The signal outgoing from the photomultiplier, may be regarded as a superposition of many signals caused by single photoelectron incident on to the first dynode. The distribution of these electrons is described by equation 1.2. Therefore, the outgoing signal is an integral convolution of a scintillator pulse and a photomultiplier response to the single electron.

$$I(t) = \int_0^t i(t - t') \cdot SER(t') \cdot dt' \tag{1.7}$$

where SER(t) - the single electron response
i(t) - the light pulse

One of the important quantities characterizing the photomultiplier is the gain variance. In a simple minded model the production of the secondary electrons at a dynode can be assumed to be governed by a Poisson distribution. Hence, the number of electrons created on the first dynode has a mean value δ, a standard deviation $\sqrt{\delta}$ and a relative variance $1/\delta$, and so on. It could be pointed out, from the properties of the Poisson statistic, that the relative variance of the mean number of electrons col-

lected at the anode is represented by the following expression: [12]

$$\frac{\nu_G}{\overline{G}^2} = \frac{1}{\delta} + \frac{1}{\delta^2} + \cdots \frac{1}{\delta^n} \approx \frac{1}{\delta - 1} \tag{1.8}$$

Thus, the spread in the pulse amplitude is dominated by the δ fluctuation from the first dynode. This is the next reason why higher voltage is applied between the photocathode and the first dynode than between the following dynodes.

Chapter 2

The photomultiplier

2.1 Plateau

In almost all experiments with scintillation caunters the PM signal is followed by a discriminator. If the scintillator is irradiated, and the signal after the discriminator is input into a scaler, one can observe the counting rate change with the applied voltage for a specific discriminator threshold. The higher the supplied voltage, the larger the counting rate. However, one or more plateaus can be observed according to the type of the source.

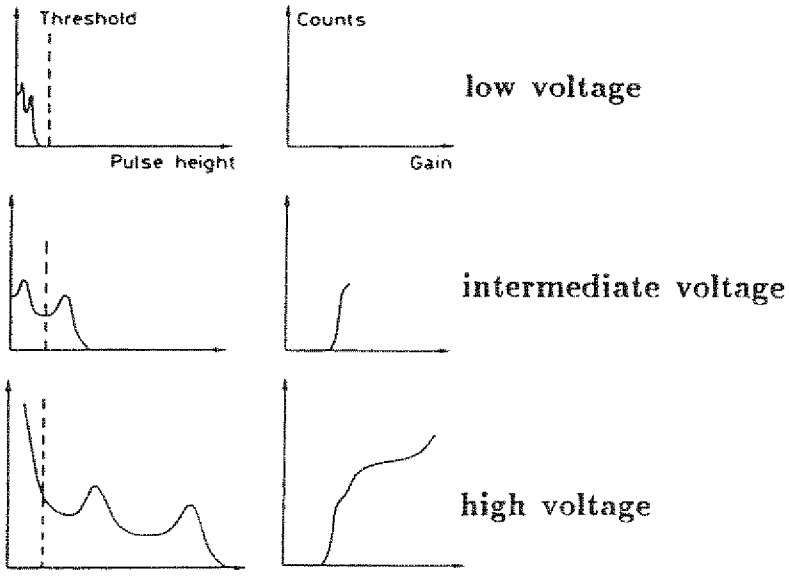

Figure 2.1 Steps leading to the scintillator counting plateau, taken from [13]

The left side of Fig. 2.1 shows a sketch of a ^{207}Bi spectrum. At a very low voltage the entire spectrum lies below the threshold value and no counts are observed. With increasing voltage more and more parts of the energy spectrum pass the threshold and are counted. Figure 2.2 shows the measured plateau for the tested detector.

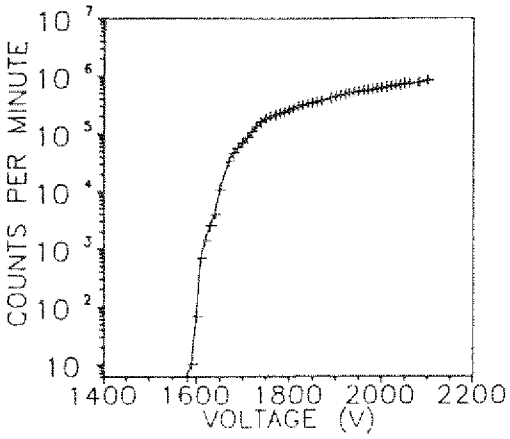

Figure 2.2 Plateou curve measured using a ^{207}Bi source

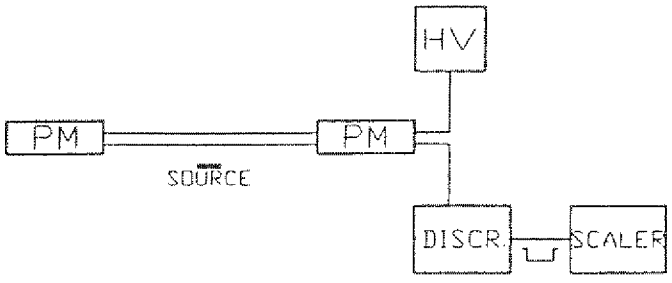

Set-up used in the measurement

2.2 Measurement of the single electron response

If only one electron hits the first dynode then the electric signal collected on the anode is called the single electron response. By measuring the charge in such signal one can deduce the photomultiplier gain. At room temperature typically thousand electrons may escape from the photocathode per second (dark current) This suggest that it would be enough to measure a photomultiplier noise charge spectrum, which should consist of one big peak from one incident electron and further much smaller peaks due to two or more electrons. However this is not the case. One is not able to distinguish any peak in such a spectrum. Unfortunately there is too large noise caused by the multiplier section. The only way to get rid of this is to trigger the electronics when a real signal is expected, even if it

is only one photoelectron. This can be performed by means of very weak light, produced by the light emitting diode [14].

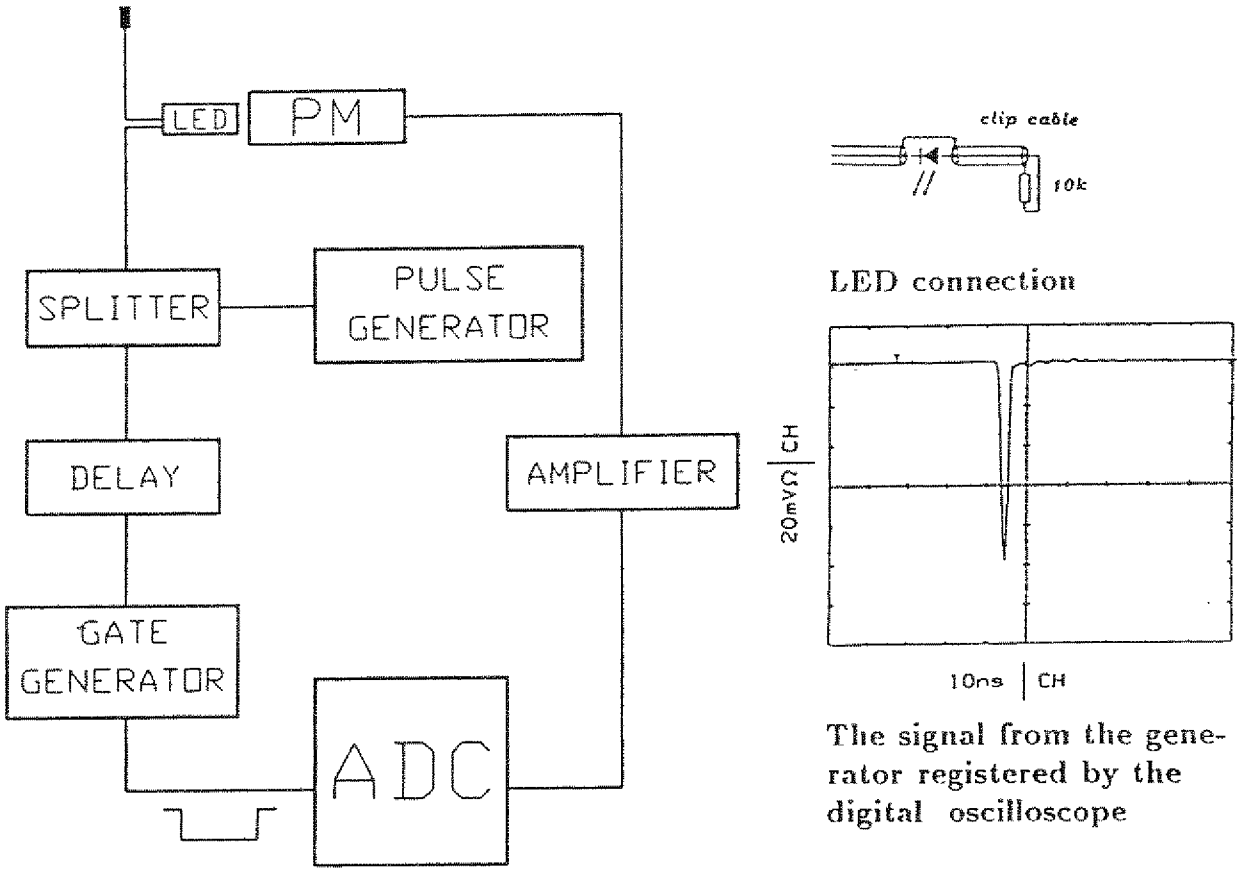

Figure 2.3 **Block diagram of the electronic system used in the single electron response measurement. ADC – analog (charge) to digital converter**

The very short pulse from a generator switches on the diode and simultaneously triggers the charge to digital converter. The signal reflected from the open end of a clip cable switches the diode off. Thus the number of photons in one pulse can be established by the amplitude of the generator signal as well as by the clip cable length. The signal from the photomultiplier first is amplified and then analized by the charge to digital converter.

In the case of the absence of the diode signal one observes in the charge spectrum a sharp peak caused by the noise of the amplifier. If a low signal is inserted into the diode producing only a few photons, a separate peak appears in the charge spectrum.

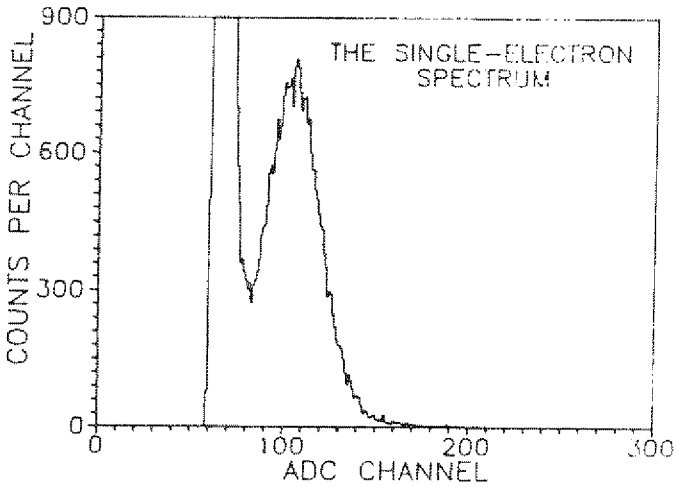

Figure 2.4 The single electron spectrum

Figure 2.4 shows a measurement with such a low diode voltage that only a single electron spectrum was observed, whereas in Fig. 2.5 the voltage was increased and a clear two-electrons peak is seen.

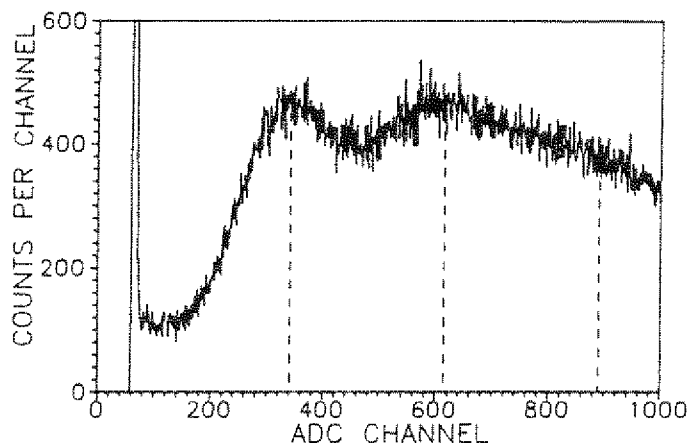

Figure 2.5 Single and two-electrons peaks

As expected, the average charge in the signals resulting from two photo-

electrons is two times larger than the charge in the single electron signal. Actually, the spectrum shown in Figure 2.5 is a superposition of a few peaks, however only the first two are clearly visible, the others have too large width to be distinguishable.

2.3 The gain variation

The number of secondary electrons emitted from the dynode depends on the energy of the electron impinging onto it. This energy is proportional to the inter-dynode potential. For that reason the gain of a photomultiplier reveals a dependence on the overall applied voltage. Measurements of

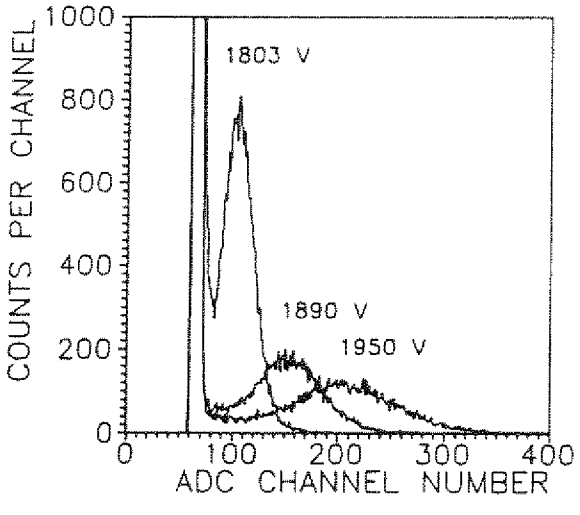

Figure 2.6 Single electron peaks measured for various supplied voltages

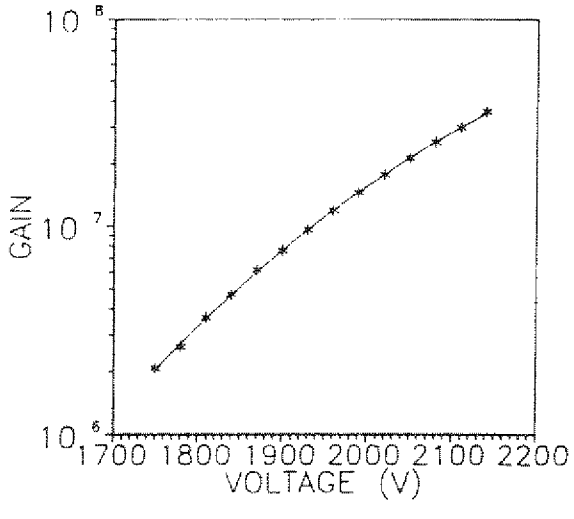

Figure 2.7 Photomultiplier gain versus supplied voltage

the single electron charge spectrum for different voltages allow to find this dependence quantitatively. To each spectrum a Gaussian function was fitted. The extracted mean value divided by the signal amplification gives directly the PM gain.

The gain variation with respect to the supplied voltage is shown in Fig. 2.7. The experimental points were fitted by a polynomial of second

degree and the following coefficients were evaluated:

$$Log(Gain) = -2.7 \cdot 10^{-6} \cdot V^2 + 1.4 \cdot 10^{-2} \cdot V - 9.4 \qquad (2.1)$$

where voltage is expressed in Volts.

Chapter 3

Methods of the detector examination

This chapter contains the description of different experimental arrangements used for measurements of *the detector response*. Methods of data evaluation are presented as well.

The output signal of the detector contains information concerning the registered particle. Usually the energy, the time when the particle passes through the detector and the hit position are of main interest. These quantities can be determined, provided the relations between them and the relevant characteristics of the pulse are known. These relations are referred to as the detector response. A method to find the specific detector response is to measure the charge and the time spectrum due to monoenergetic particles bombarding the detector at a fixed position. In large modules, as in the present case, the response function changes drastically over the detector volume. Thus, it is necessary to scan the whole detection area.

In order to examine the detection module two measuremants were performed. In the first one a collimated ^{90}Sr electron source was used, and the second was carried out at a monoenergetic proton/pion test beam of 2 GeV/c momentum.

3.1 Experimental set-up used in measurements with the ^{90}Sr source

The response of a scintillation counter of dimensions 450 x 100 x 4 mm^3 was examined. For the measurements an additional scintillation detector (see Fig. 3.2) was used, which served as a start counter and analyzer of the electron energy. An electron, in order to be registered in the present electronic logic, has to have enough energy to pass through the tested detector and to produce a signal, in a start counter, higher than the threshold in the discriminator-2 and smaller than the threshold in the discriminator-1, see the electronic diagram in Fig. 3.2. In this manner electrons from a narrow energy strip were selected from a continuous β spectrum. This allows

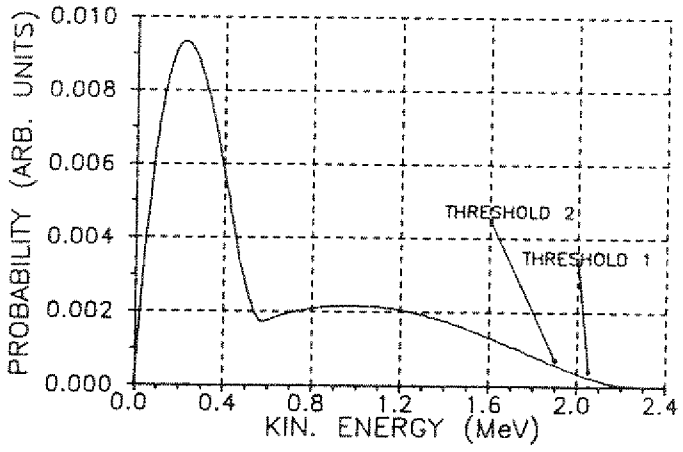

Figure 3.1 The emission spectrum of a ^{90}Sr β - source

to study the relative pulse charge changes along the scintillator surface.

After leading edge discrimination the timing of the pulses is arranged as shown in Fig. 3.2. The signal from the start detector is delayed so much that its leading edge comes as the last one, but has an timing overlap with the broader signals from the tested module. Therefore it is correlated, in time, with a coincidence pulse. Such an adjustment provide that the TDC unit is always started at the same time with respect to the hit moment.

The simultaneous registration of charge and timing of a signal enables

to reduce shifts in the time spectra caused by the "time walk" of the discriminators (see section 3.4).

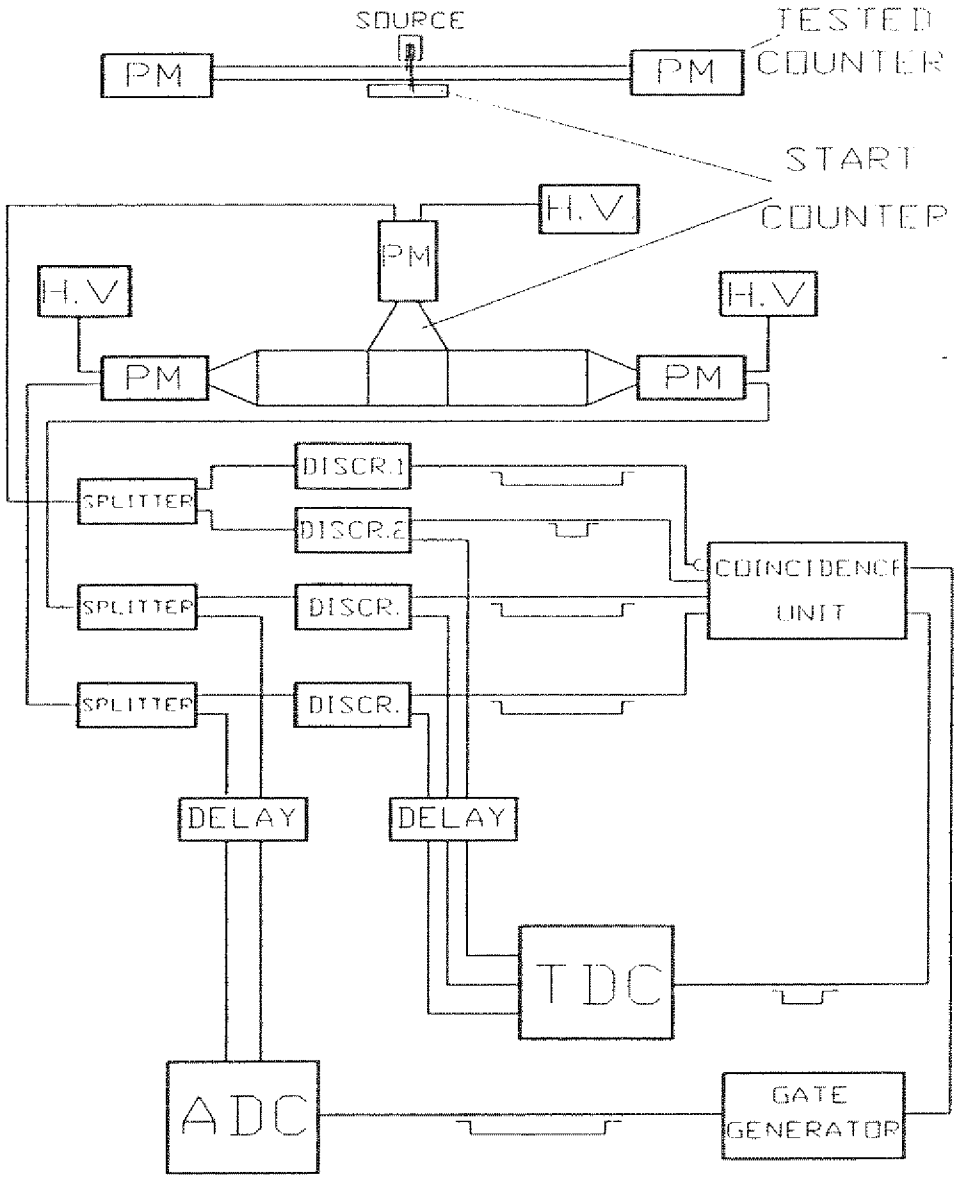

Figure 3.2 **The experimental set-up together with the block diagram of the electronic system.**
ADC – analog (charge) to digital converter,
TDC – time to digital converter

3.2 The experimental set-up used in the measurement at a proton and pion beam

In this experiment the response of the detection module was tested with minimum ionizing pions and protons of the test beam T11 at CERN.

The event was accepted if a particle passed through the start and the stop counter. The hit position was defined by means of two delay wire chambers (D1,D2) with an active area of 10 cm x 10 cm. The initial particle momentum was 2 GeV/c $\pm$ 20 MeV/c. The difference in time of flight between protons and pions equals to 4.36 ns, for the distance between the start and stop counter. This allowed to separate pions and protons by a time of flight measurement.

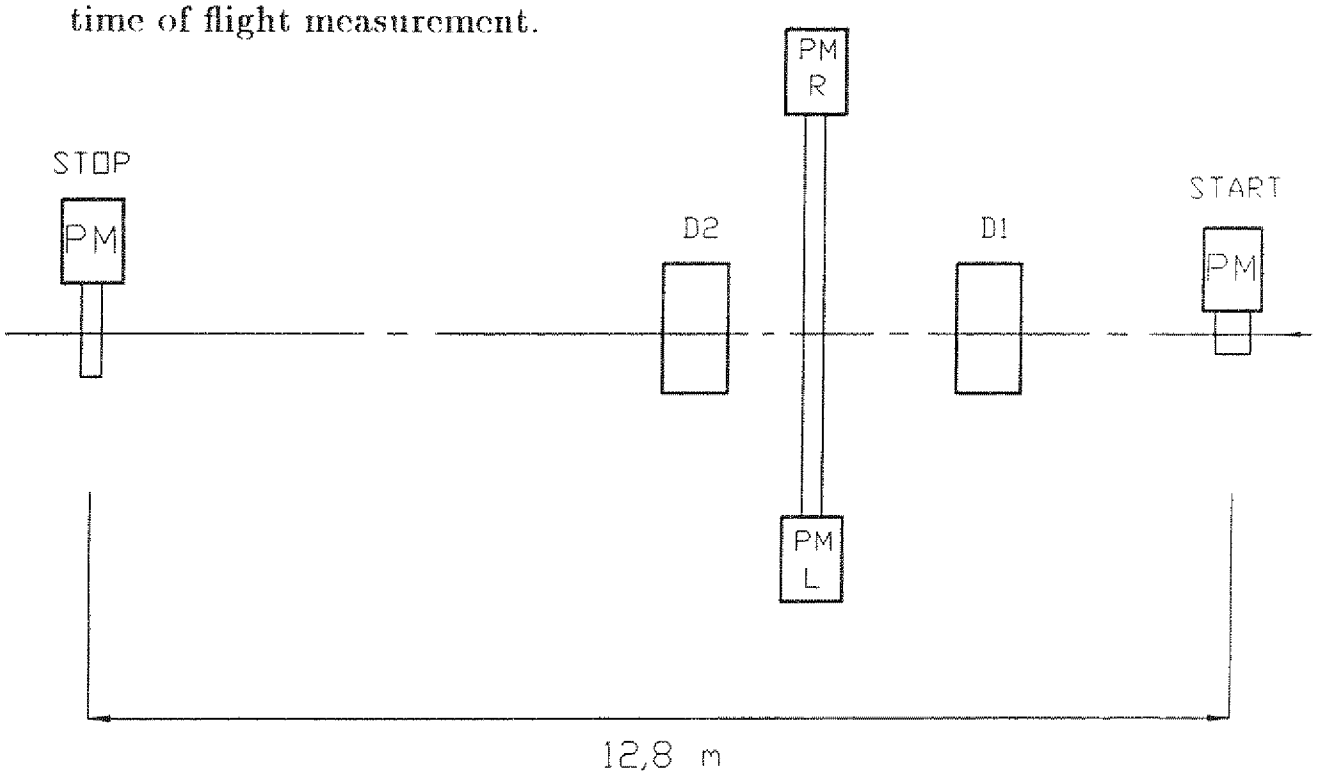

Figure 3.3 Schematic view of the experimental arrangement
D1,D2 — delay wire chambers
START – 4 cm x 4 cm scintillation counter
STOP — 10 cm x 10 cm scintillation counter

The beam was incident normal to the tested counter with an angular acceptance of ~ 6 mrad and ~ 20 mrad for horizontal and vertical direction, respectively. During the experiment the position of the detector was changed a few times in order to investigate the entire scintillator area. For each photomultiplier output the integrated charge of the pulse and the time of the pulse arrival were registered. The latter was measured in reference to the common timing determined by the stop counter.

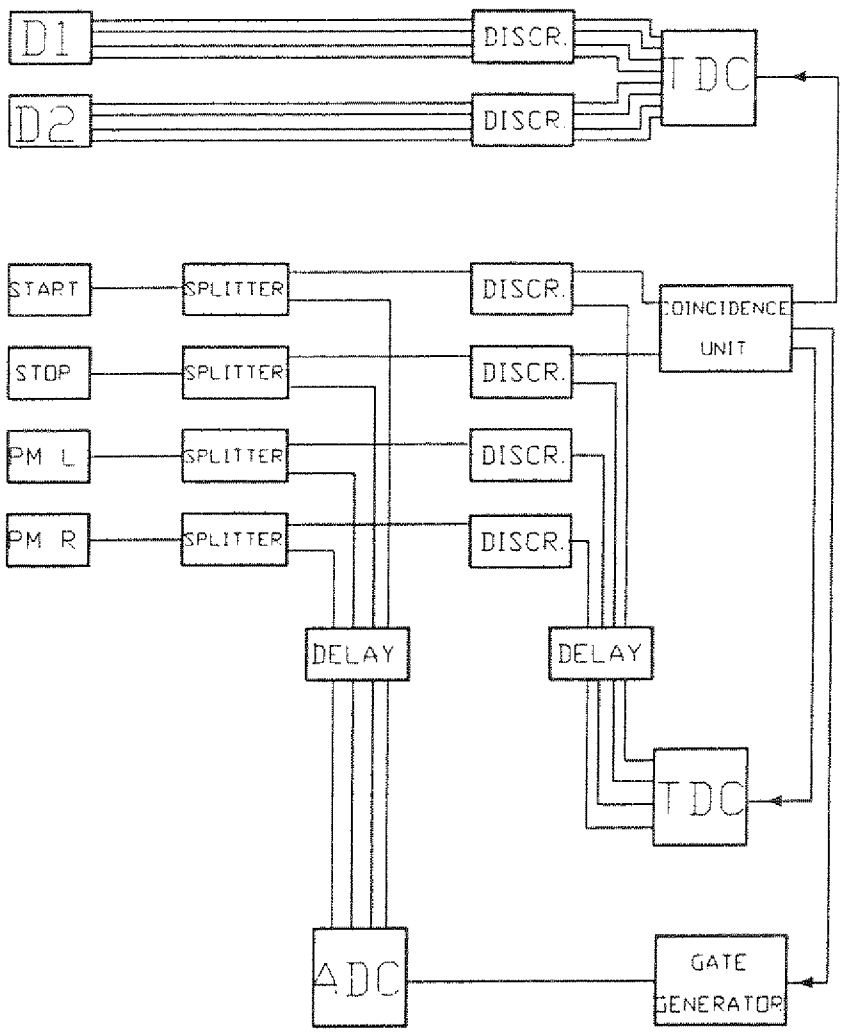

Figure 3.4 Block diagram of the electronic system

3.3 Hit position determination

Each delay wire chamber provides four timing signals ($t_{up}, t_{down}, t_{left}, t_{right}$), which carry information of the impact position of the particle [15]. The time differences $t_{up} - t_{down}$ and $t_{left} - t_{right}$ define vertical and horizontal coordinates of the hit point relative to the center of the chamber, respectively.

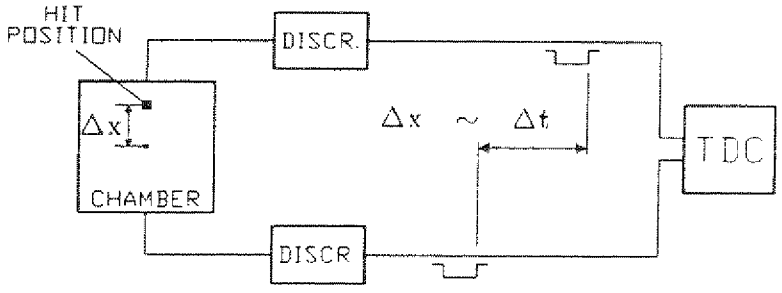

Figure 3.5 The position determination by the delay wire chamber

In one of the measurements the scintillator was adjusted such that it was covered by part of a beam only (see Fig. 3.6). This allowed to define the position of the tested detector with respect to the chambers.

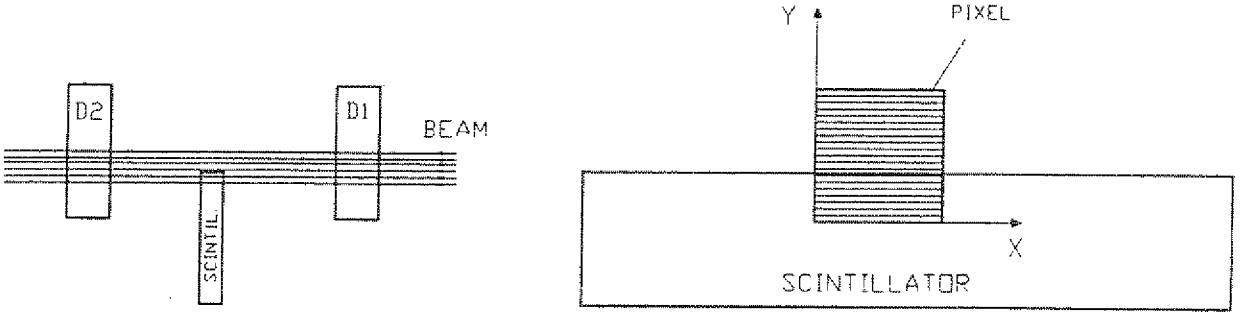

Figure 3.6 The detector position determination

The active area of the chamber was off-line divided into elongated pixels parallel to the scintillator side (see Fig 3.6). For each of them the number of events were counted for both: i) if a coincidence between chamber and tested module was observed and ii) if chambers independently of the tested module had a signal. Further, the ratio of case i) to case ii) was

extracted. Ideally unity was expected for pixels corresponding with the area of the tested detector, and zero for the rest.

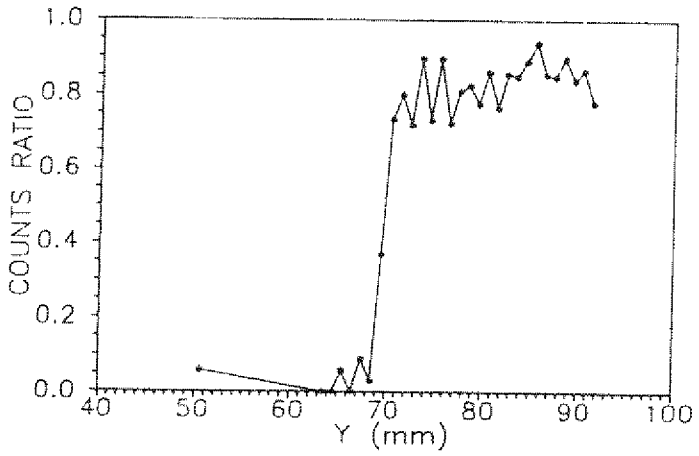

Figure 3.7 Upper scintillator side in relation to the chamber D2

Thus, the scintillator edge is defined with an accuracy of ± 1 mm (see Fig. 3.7). The shifts of the detector during the experiment were done with the same precision. As a result the overall resolution of the hit position determination amounts to ± 2 mm (FWHM). The fact that an efficiency of only $\sim 80\%$ is observed can be explained by accidental coincidences of the chambers.

3.4 Time walk correction

An analog output pulse from a detector is converted into a logic signal by a discriminator. The most common method for deriving a timing signal, employed also in the present case, is *leading edge triggering* (Fig. 3.8). The logic signal, in this technique, is generated at the moment the analog pulse crosses the threshold (Fig. 3.8). As one can see, out of two pulses having the same rise time, the higher crosses the threshold earlier. Therefore, even exactly coincident signals may trigger the discriminator at different times. This is refer to as a *time walk effect.*

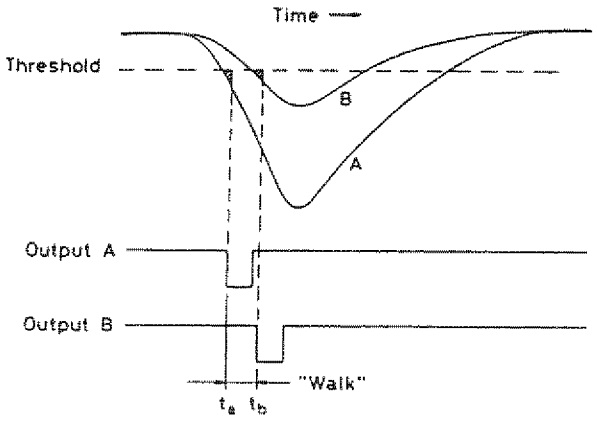

Figure 3.8 Walk in a discriminator, taken from [13]

The variation in the amplitude of the incoming pulses is not the only source of the discriminator walk. The other one is the finite amount of a charge needed to trigger the discriminator, indicated by the shaded areas in Fig. 3.8.

Quantitatively the time walk effect is represented by [16]:

$$\Delta t = const. + \beta \cdot \frac{1}{\sqrt{q}} \tag{3.1}$$

where q is the amplitude of a pulse, and β is a coefficient determined by the data. Thus the walk corrected time t is expressed by:

$$t = const. + t' - \beta \cdot \frac{1}{\sqrt{q}} \tag{3.2}$$

where t' is a measured time.

The walk is clearly seen in a scatter plot (Fig. 3.9a), which shows a relation between t' and $\frac{1}{\sqrt{q}}$. Here t' stands for the time of flight between the stop and the tested counters, whereas q represents the integrated charge of the signal from the tested detector. As expected, for pulses (from the tested detector) with higher amplitude the discriminator generates the logic signal earlier, hence the measured time of flight is longer.

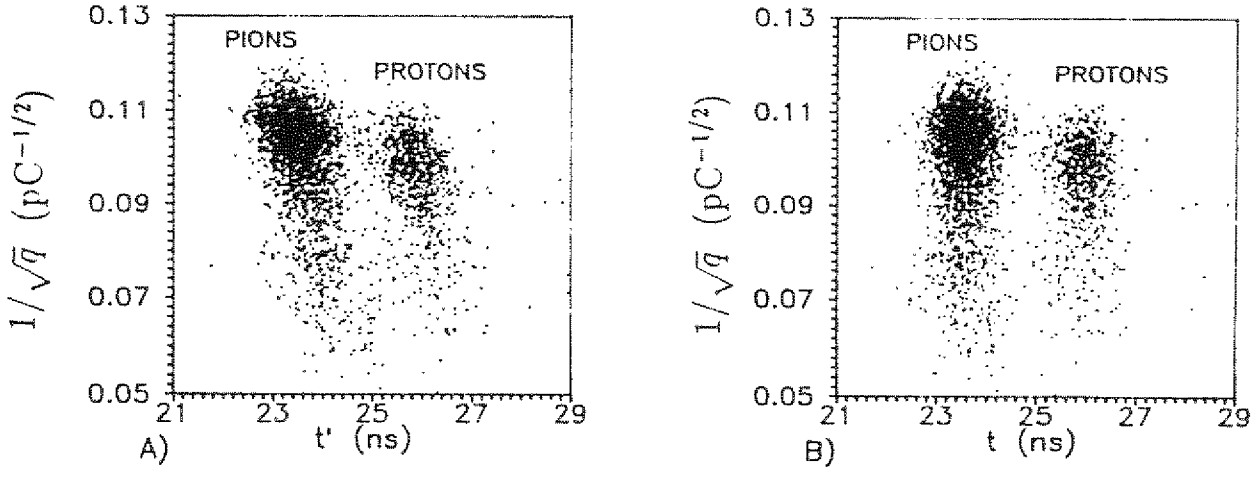

Figure 3.9 An example of the scatter plot t vs. $\frac{1}{\sqrt{q}}$ measured at the center of the detector, A) before, B) after time walk correction

For long scintillation counters the shape and the amplitude of the pulses depend on the hit position. Therefore the parameter β in equation 3.1 may reveal position dependence. Table 4 shows this coefficient evaluated for a few points on the scintillator.

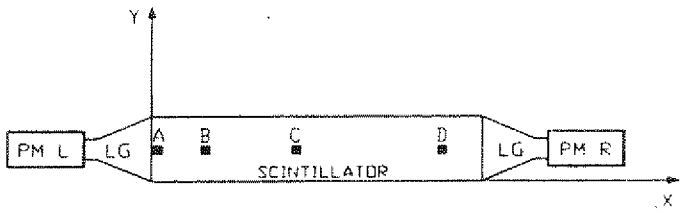

Table 4.

β value [ns·pC$^{1/2}$]		position
PM R β_R	PM L β_L	
-16.6	-16.1	A
-17.4	-13.0	B
-20.5	-15.2	C
-19.5	-14.2	D

As no regularity can be found in β variations, it is assumed to be constant over the entire scintillator surface. In further considerations β is taken as a mean value of the numbers in table 4, with the error being a standard deviation of the mean. Evaluated β values amount to: $\beta_R = -18.5 \pm 1.8$ ns·pC$^{1/2}$ and $\beta_L = -14.6 \pm 1.3$ ns·pC$^{1/2}$. The inaccuracy

in determining this coefficient implies that the error of the walk correction ($\sigma_{\Delta t} = \sigma_\beta \cdot 1/\sqrt{q}$) is as high as 200 ps for low signals (see Fig. 3.9).

3.5 Particle identification

Pions and protons, used in the experiment had the same momentum of 2 GeV/c. However, because of different masses, they had different velocities given by:

$$v = \frac{p \cdot c^2}{E} = \frac{pc}{\sqrt{p^2 + m_0^2 \cdot c^2}} \tag{3.3}$$

where c is the light velocity and m_0,p are the rest mass and momentum of a particle, respectively. This relation results in the time of flight difference of the particles being considered as 341 ps per meter. Thus, the distance of 7 m between the stop and the tested detector is equivalent to 2387 ps.

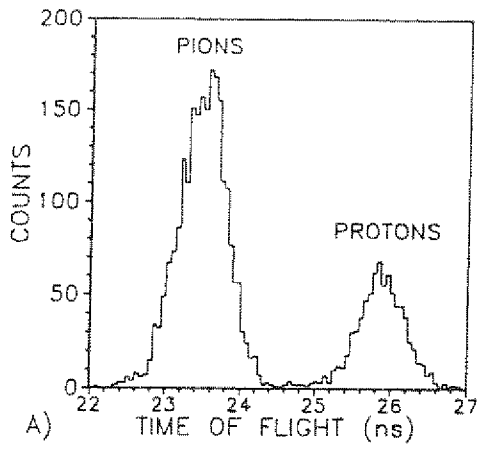

Figure 3.10 Time of flight spectrum

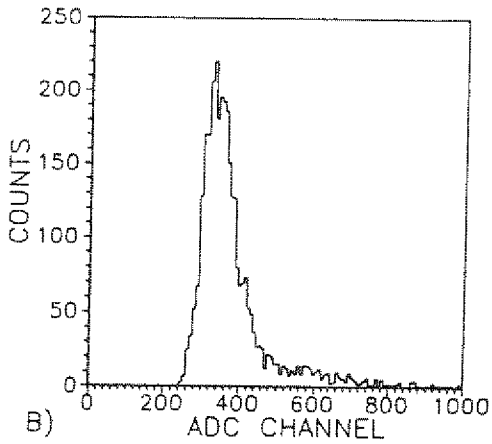

An example of ADC spectrum for the tested detector

Figure 3.10A shows a walk corrected time of flight spectrum between these counters. As expected, very well separated peaks are observable.

To complete the considerations concerning the data evaluation, a typical ADC spectrum is shown in Fig. 3.10B. Unlike in the TDC spectra, here protons and pions are indistinguishable. This is because their energy loss is nearly the same.

Chapter 4

The response of the detection module

The coordinate system referrd to in the next sections is defined as:

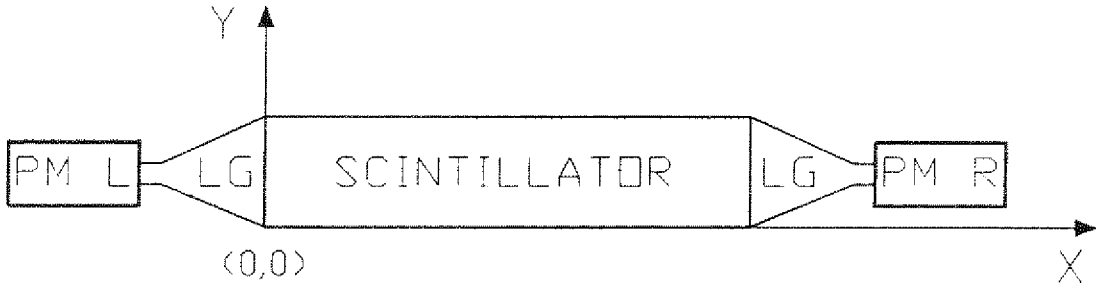

Figure 4.1 Definition of the coordinate system

4.1 The detector efficiency

One of the main detector characteristics is its efficiency. This is defined as that fraction of events impinging on the detector, which is registered. An efficiency is a function of radiation type, energy and of the detector material. This is because no material is equally sensitive to all radiation kinds, and the sensitiveness of each material changes with the given radiation energy.

In order to be registered a particle has to produce a signal, which is high

enough to exceed a necessary discriminator threshold. The signal height is associated with the number of photons generated in the scintillator, which is proportional to the energy deposited by the particle. Thus the efficiency can be expressed as the probability of producing enough photons to generate a signal higher than the threshold.

For a monoenergetic beam the variations in the number of produced photons is governed by the Poisson distribution. Consequently the efficiency can be approximated by:

$$E = \sum_{r=th}^{r=\infty} \frac{\mu^r \cdot e^{-\mu}}{r!} \tag{4.1}$$

where th is the number of photons equivalent to the 'threshold pulse' and μ is the average number of produced photons.

Minimum ionizing particles deposit about 0.7 MeV in a 4 mm thick scintillator. The average energy required to produce a scintillation photon is a fixed number dependent only on the scintillator material. In plastic scintillators it amounts to about 100 eV per produced photon [17]. Assuming (in the worst case, see section 4.3) the light collection efficiency 7%, and the photocathode efficiency 25% one can calculate that on the average 122 photoelectrons are generated.

$$7 \cdot 10^5 eV \longrightarrow \sim 7 \cdot 10^3 \frac{scintillation}{photons} \longrightarrow \sim 122\ photoelectrons$$

At normal parameters used for the photomultiplier one photoelectron gives a signal with a height in the order of 40 mV. Therefore, a signal caused by 5 photoelectrons easily exeeds the discriminator threshold of typically 50 mV. In the case being under consideration 5 photoelectrons are equivalent to ~ 286 scintillation photons. Taking in equation 4.1 th $= \sim 286$ and $\mu = \sim 7000$ one obtains the efficiency better than 99.99%. Moreover, the efficiency of the scintillation counters for minimum ionizing particles detection remains constant down to a scintillator thickness of ~ 0.3 mm. Then μ is equal to ~ 525.

4.2 A pulse charge variation

Although in ternary scintillators self absorption is relatively small, for long detectors it influences significantly the light collection process. Therefore, for scintillators of dimensions comparable to the bulk light attenuation length one observes a variation of the pulse height depending on the irradiated position, even for monoenergetic particles.

In long scintillators the photons normally make a lot of reflections before they reach the edge coupled to the light guide. Thus, the bulk light attenuation is not the only factor causing changes of the signal height. The other one is the reflection loss at a scintillator surfaces.

These factors result in a light attenuation described by:

$$N = N_0 \cdot e^{-\frac{x}{\lambda_t}} \tag{4.2}$$

where λ_t is called a technical light attenuation length, and N_0, N are the number of collected photons when the scintillator is irradiated at X = 0 and x, respectively. Figure 4.2 shows the relative photomultiplier

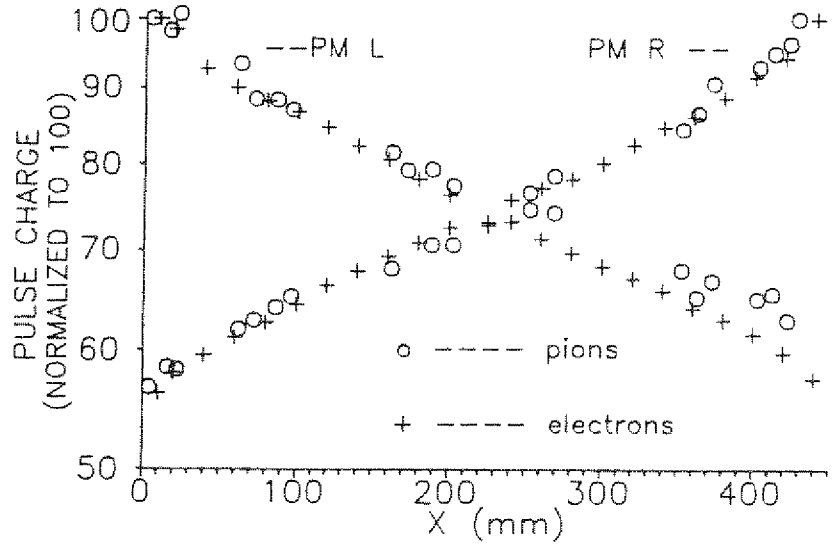

Figure 4.2 Relative variations in the signal charge for 2 GeV/c pions and for electrons from a ^{90}Sr source

pulse charge variations according to the position along the line connecting the photomultipliers. The signal charge was evaluated as a mean value of a Gaussian distribution fitted to each ADC spectrum. By fitting a line to the experimental points (shown in Fig. 4.2), without taking the data at the ends of the scintillator into account, the technical light attenuation length was found to be equal to 88 cm ± 5 cm.

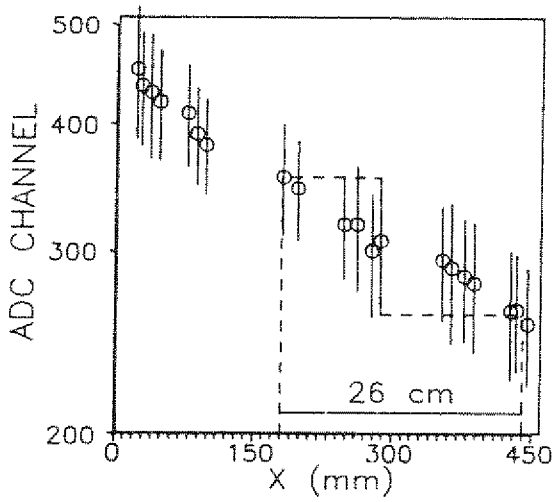

Figure 4.3 A rough position determination

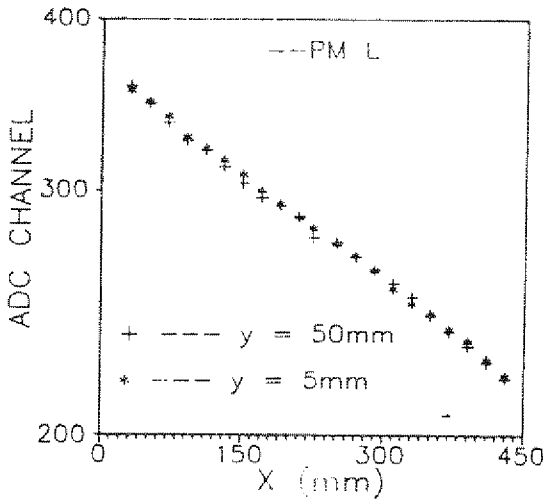

Figure 4.4 Pulse charge dependence on the y-coordinate

The considerable variation of the charge from the pulse in the x-direction allows to estimate roughly the x-coordinate of the hit position. Figure 4.3 shows the signal charge expressed in ADC channels, together with the estimated error of a single measurement (σ of a Gaussian distribution). From this figure one can derive that the error of determining the hit position amounts to ± 13 cm. Taking into account, however, that in the actual experiment the scintillator will be read out simultaneously by two photomultipliers this value will reduce to ± 9 cm.

In contrast to the pulse height variation in the x-direction, there is essentially no dependence on the y-coordinate (see Fig. 4.4).

Similar tests of pulse charge changes with respect to the hit position were performed with two other scintillation detectors, which are shown

schematically in Fig. 4.5. As can be seen, a scintillator with read out on both ends reveals, in one photomultiplier, much larger pulse height variations in comparison with those read out on one edge only. This is because in the latter the light reflected from the sicintillator edge (opposite to the end glued to the light quide) also contributes to the signal amplitude.

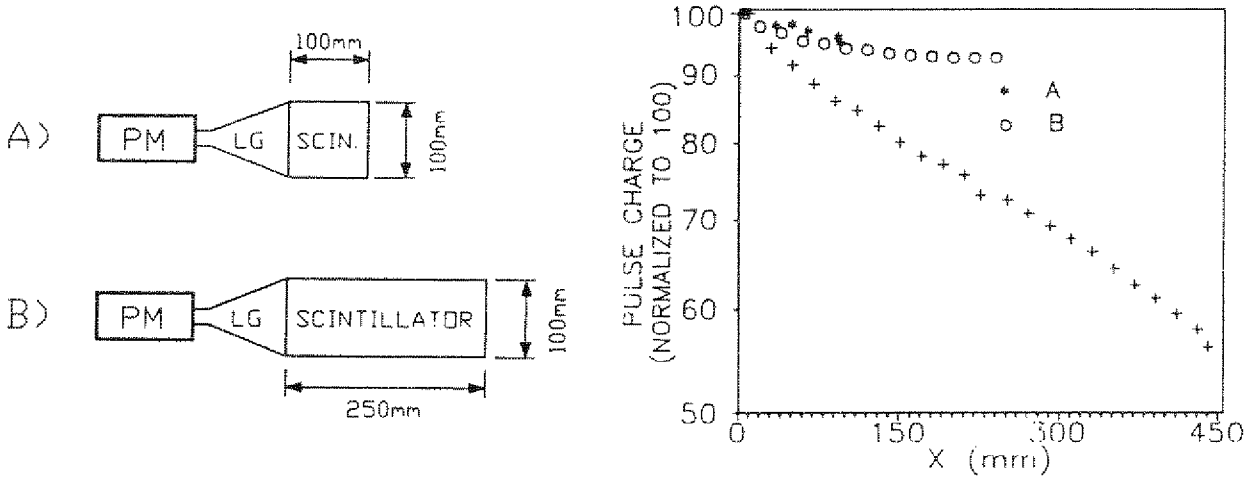

Figure 4.5 Comparison of pulse charge changes for various detectors

4.3 Estimation of the light collection efficiency

The considerations in this section concern the measurements performed with a ^{90}Sr electron source.

Dividing the integrated charge of the signal by the photomultiplier gain one can calculate the number of photoelectrons generated in the photocathode (see Fig. 4.7), which allows to estimate the number of photons reaching the photomultiplier. On the other hand one can estimate the number of photons produced by the registered particle in the scintillator.

Electrons when passing through matter suffer a collisional and radiational energy loss. However, at energies of a few MeV or less the latter can be neglected. Figure 4.6A shows the ionization energy loss per unit length, for electrons in a scintillator material, derived from the Bethe-Bloch[1] for-

[1]coefficients for plastic scintillators can be found in [13] on page 26

mula. This relation allows to calculate (numerically) an average energy loss from electrons within the scintillator medium of the tested detector.

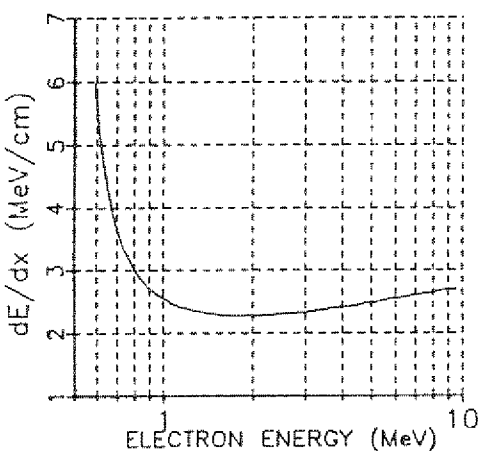

Figure 4.6 A. The stopping power dE/dx as a function of energy for electrons [18]

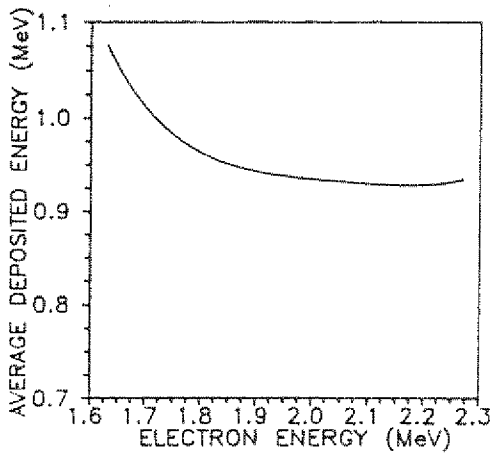

B. Average energy deposited by electrons within a 4mm thick scintillator versus its energy

By a suitable threshold adjustment, from the continuous β spectrum, only electrons of an energy about 2 MeV were registered. Due to the low energy resolution of the scintillator the energy of the measured electrons is not very well defined. However, the energy deposited by electrons of an

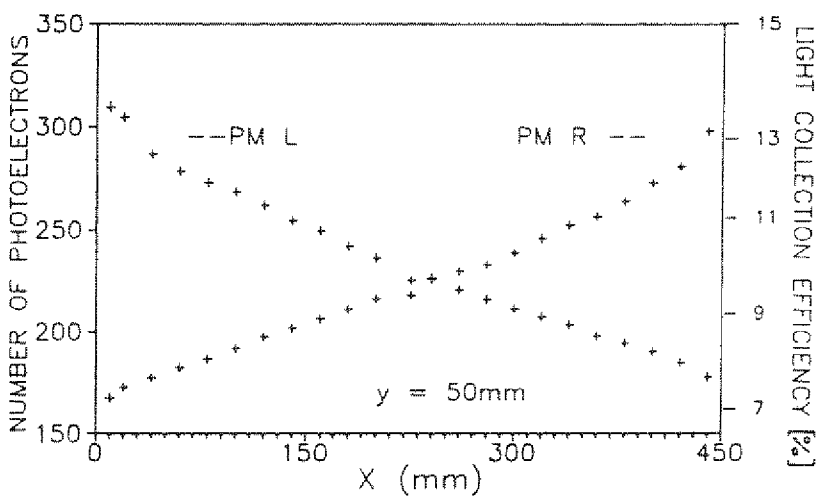

Figure 4.7 Number of electrons on the first dynode and light collection efficiency as a function of the position in a scintillator

energy larger than 1.9 MeV is nearly constant and amounts to ~ 0.93 MeV (see Fig. 4.6B). Thus, on the average one electron produces 9300 fluorescence photons. Hence, dividing the number of photoelectrons by 9300 and by the photocathode efficiency (0.25) one obtains the light collection efficiency (see Fig. 4.7). For one photomultiplier this varies, depending on the hit position, from $\sim 7\%$ to $\sim 13\%$. Consequently, the fraction of fluorescence light seen by both photomultipliers amounts to $\sim 20\%$ independently of the hit position in the scintillator.

4.4 The light pulse velocity

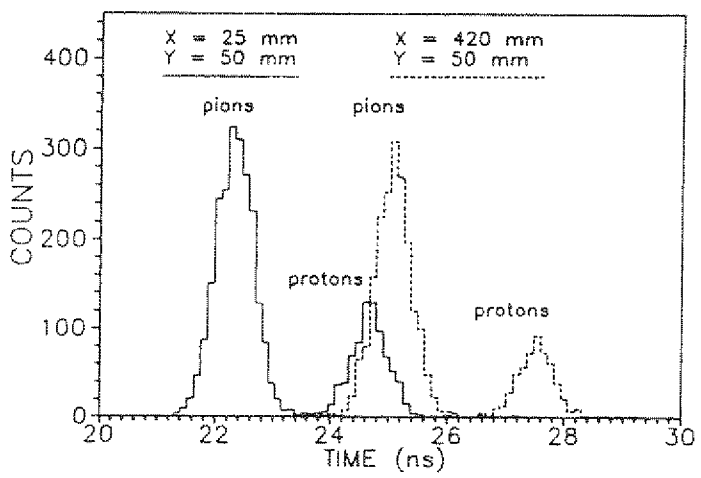

Figure 4.8 Time of flight spectra between the stop and the tested counter, for two different beam positions, measured with 2 GeV protons and pions

Figure 4.8 shows that the time of the signal arrival at a TDC unit depends on the x-coordinate of the impact position. Thus, in order to establish the time when the particle strikes the detector, it is necessary to know the hit position as well as the effective velocity of the light pulse in the scintillator. In experiments at the COSY ring the former will be provided by the drift chambers (see Fig. 0.1).

The mean value of the Gaussian distribution fitted to each spectrum is calculated with a very small error in the order of 7 ps, which is defined

as $\sqrt{\nu/n}$, where ν is the variance of a distribution and n is a number of events. Unfortunately, the TDC peaks are shifted because of the time walk in the discriminator. This shift varies over the scintillator surface, since the average signal height depends on the position. Thus, in order to measure the real time differences between the TDC spectra originated in different positions, the time walk has to be corrected. Inaccuracy of this correction estimated in chapter 3.4 amounts to values as high as ± 200 ps (σ) for low signals.

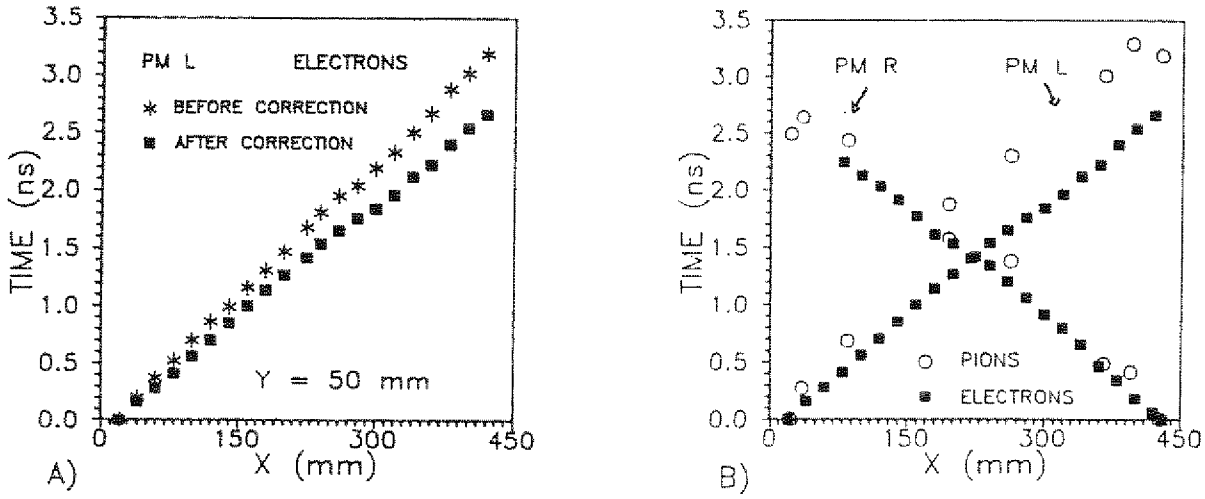

Figure 4.9 **Variation of the TDC peak with respect to the hit position.**
A. For electrons before and after time walk correction,
B. For electrons and pions after correction
Time is measured in relation to the timing of the signal produced at x = 25 mm for PM L and at x = 425 mm for PM R

By fitting a line to the measured points the light signal velocity was found to be:

Table 5.

Light pulse velocity [cm/ns]	Measurements with:	
15.5 ± 0.6	PM R	^{90}Sr
15.3 ± 0.6	PM L	source
15.9 ± 0.8	PM R	pions and
12.3 ± 0.6	PM L	protons

The first three values in Table 5 are equal within the error limits, whereas the velocity measured by means of PM L at p and π^+ beam differs from the rest. This discrepancy might have been caused by a wrong TDC calibration or by pedestal variations during the measurements. Since the experimental set-up is dismounted further inspection is not possible.

T. Tanimori et al. [16] examined a similar scintillation detector. They obtained the effective light velocity of 16.3 ± 0.2 cm/ns for 2 cm thick scintillator and 16.7 ± 0.2 cm/ns for the 3 cm thick one.

4.5 Time resolution

Fluctuations of the signal timing are caused mostly by a walk and a jitter. The former can be corrected by the data analysis, conversely, the jitter arising from the intrinsic detection processes can not be avoided. Because of this even two exactly coincident signals do not give the same time. More over, the accuracy of currently available TDC units is not better than 25 ps per channel. Thus, to take advantage of the signal timing, the system (detector + electronics) time resolution has to be estimated. This was done by measuring the distribution of the time differences between signals from PM-L and PM-R, generated by the same particle. Ideally it should be a δ-function, but obviously it is not the case, in fact its width changes with irradiated position. A typical distribution for $\Delta t = t_R - t_L$, together with the fitted Gaussian function, is shown in Fig. 4.10. The variance of this distribution resulting from fluctuations of the signal timing from the two photomultiplies is expressed by:

$$\nu = \sqrt{\sigma_{t_R}^2 + \sigma_{t_L}^2} \tag{4.3}$$

where, $\sigma_{t_R}^2$ and $\sigma_{t_L}^2$ are the standard deviations in determining t_R and t_L, respectively. In order to establish the overall time resolution of the tested detector this variance has to be combined with the error of a walk correction.

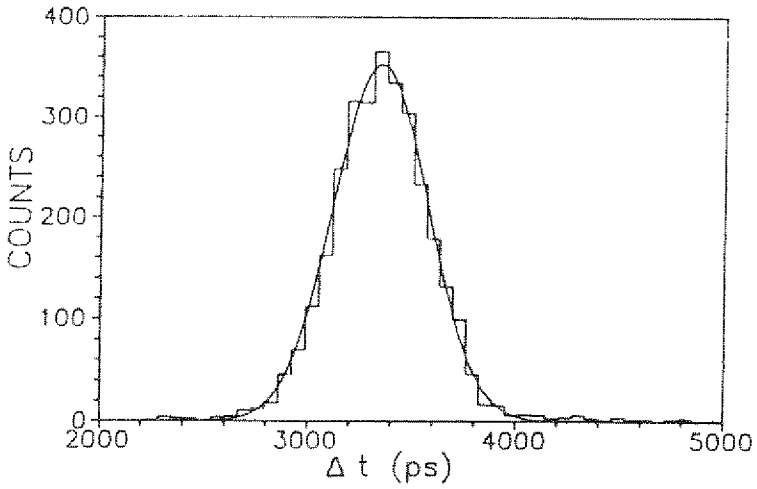

Figure 4.10 An example of a Δt spectrum measured at x = 25 mm

The relation between the measured hit time and the actual one is as follows:

$$t_L = t^L_{measured} - \Delta t^L_{walk} + (\frac{x}{v_{eff}}) + const.$$
$$t_R = t^R_{measured} - \Delta t^R_{walk} + (\frac{L-x}{v_{eff}}) + const. \qquad (4.4)$$

where, x is the hit position, and L is the scintillator length. The "start" moment for the time of flight measurement between the S1 and S3 detectors (see Fig. 0.1) in the COSY - 11 (E-5) experiment will be defined as a mean value of t_L and t_R.

$$t_{start} = \frac{t^L_{measured} + t^R_{measured} - \Delta t^L_{walk} - \Delta t^R_{walk}}{2} + const. \qquad (4.5)$$

This implies that

$$\sigma^2_{t_{start}} = \frac{\sqrt{\sigma^2_{t_L} + \sigma^2_{t_R} + \sigma^2_{\Delta t^L_{walk}} + \sigma^2_{\Delta t^R_{walk}}}}{2} \qquad (4.6)$$

Term $\sigma^2_{t_L} + \sigma^2_{t_R}$ is equal to the variance of the $\Delta t = t_L - t_R$ distribution, which reveals a dependence on the irradiated position. Similarly the standard deviation of a time walk correction ($\sigma_{\Delta t_{walk}}$) is a function of a signal height (see section 3.4), hence depends on the hit position. Consequently, the evaluated value of $\sigma_{t_{start}}$ (shown in Fig. 4.11) is not constant over the scintillator surface.

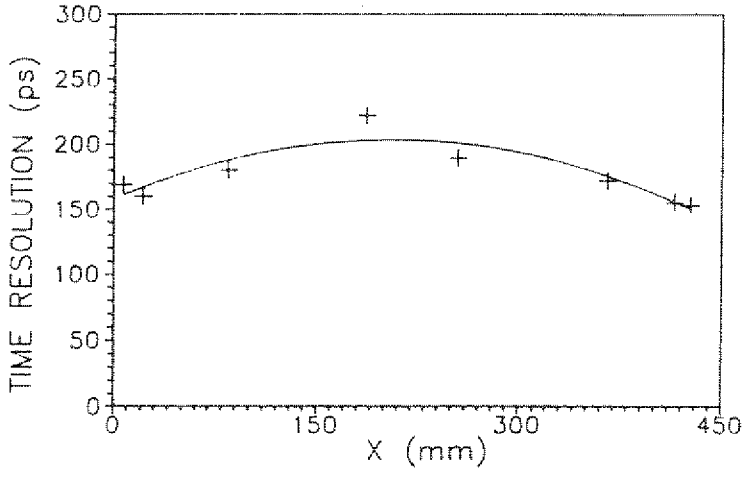

Figure 4.11 The overall time resolution of the tested detector for a few points in the scintillator. The curve is drawn to guide the eye

This estimation shows that the error of determinig t_{start} varies from ~ 160 ps at the scintillator edges to ~ 220 ps at the centre. Furthermore, for the resolution of a time of flight set-up, this approximated $\sigma_{t_{start}}$ has to be folded with the time resolution of the stop counter.

Acknowledgements

I would like to thank to Prof. L. Jarczyk and Prof A. Strzałkowski for supporting my work, and also to Prof. K. Kilian and Dr. hab. W. Oelert for enabling me study in the Nuclear Institute of the Forschungszentrum Jülich. I am especially grateful to Dr. hab. W. Oelert for guiding me during my work, and for making my participation in measurements at CERN possible.

I owe a great debt to Dr. D. Grzonka and Dr. T. Sefzick for introducing me into the technique of measurements, and for their kind answers to my continual questions.

I wish to record my thanks to J. Thimmel and M. Wolke for many stimulating discussions, and also to A. Misiak and J. Majewski for their help in dealing with electronics apparatus.

Dr. M. Ziolkowski and K. Pysz were very kind in showing me how to use some programs necessary in my work.

I would like to thank the many people who have helped me in many other ways. In particular I am indebted to: Dr. R. Bröders, M. Dahmen, K. Dickinson, Prof. Ben Gibson, M. Kistryn, Dr. S. Kistryn, M. Rook, Dr. E. Roderburg, R. Stratmann, Dr. A. Szczurek and P. Żołnierczuk.

Finally my very special thanks are due to Dr. hab. W. Oelert and Dr. D. Grzonka for having read the text of the work and for their helpful comments and corrections.

References

[1] W. Oelert, *Threshold Measurements at the Experiment COSY - 11*,
Talk presented at the 105. WE - Heraeus -Seminar,
KFA - IKP(I) - 1993 - 1.

[2] Kay Königsmann, *New Hadronic states*,
CERN-PPE/91-160, 1991.

[3] BICRON, *Premium Plastic and Liquid Scintillators*,

BICRON, *Plastic Scintillators a Survey*,
by C.R. Hurlbut, 1985.

[4] J. B. Birks, *The Theory and Practice of Scintillation Counting*,
Pergamon Press, London, 1964.

[5] B. Bengston, M. Moszynski, *Study of Primary Energy Transfer Process in Ultrafast Plastic Scintillators*,
Nucl. Instr. and Meth. 155 (1978) 221-231.

[6] M. Moszynski, B. Bengston, *Light Pulse Shapes From Plastic Scintillators*,
Nucl. Instr. and Meth. 142 (1977) 417-434.

[7] M. Moszynski, B. Bengston, *Status of Timing with Plastic Scintillation Detectors*,
Nucl. Instr. and Meth. 158 (1979) 1-31.

[8] Röhm GmbH, *Datenblatt Plexiglas*,
Darmstadt, 1985.

[9] G. Keil, *Design Principles of Fluorescence Radiation Converters*,
Nucl. Instr. and Meth. 87 (1970) 111-123.

[10] L. Thornhill, *Scintillation Counter Technology*,
Geneva, 1983, SB/AC/ST/3173.

[11] THORN EMI, *Photomultipliers*, 1986

[12] Glenn F. Knoll, *Radiation Detection and Measurement.*

[13] William R. Leo, *Techniques for Nuclear and Particle Physics Experiments*, Springer - Verlag Berlin Heidelberg, 1987.

[14] T. Sefzick et al., *A system for Simulation of Scintillator Light Signals*, Nucl. Instr. and Meth. in Phy. Re. A288 (1990) 571-573.

[15] A. Marin, G. Vismara, *The Delay Wire Chamber Description*, CERN - LEP Division LEP/BI-TA/Note 85-3.

[16] T. Tanimori et al., *A Test of 150 cm x 20 cm Wide Time-of-Flight Scintillation Counters*, Nucl. Instr. and Meth. 216 (1983) 57-65.

[17] Particle Data Group, *Review of Particle Properties*, Physical Review D45, Part2, 1992.

[18] A. Empl, *Untersuchung eines Szintillation - Detektors besonderer Form*, Diplomarbeit, Bonn, 1989.

Further Reading

A. Budzanowski et al, *COSY - 11 Detector Arrangement* KFA-IKP, Jül-2590, 41.

L. Jarczyk et al., *Reconstruction of the Shape of Meson Resonances Produced in the $pp \rightarrow ppM$ Reaction Near Threshold*, KFA-IKP, Jül-2590, 43.

M. Moszynski, *Study of Light Collection From Cylindrycal Scintillators*, Nucl. Instr. and Meth. 734 (1976) 77-85.

J. B. Birks, *Energy Transfer in Organic System*, J. Phys. B (Proc. Phys. Soc), 1968, Ser. 2, vol. 1.

E. Gatti, V. Svelto, *Review of Theories and Experiments of Resolving Time with Scintillation Counters*, Nucl. Instr. and Meth. 43 (1966) 248-268

T. Sugigate et al., *100 cm long Time-of-Flight Scintillation Counters with RMS Resolution of 50 ps*, Nucl. Instr. and Meth. in Phy. Re. A249 (1986) 354-360.

LECROY, *Research Instrumentation Catalog*, 1992.

Jül-2825
October 1993
ISSN 0944-2952